A novel current mode operating beam counter based on not preamplified HPDs

M.C. Fujiwara [a], M. Marchesotti [b,1]

[a] *University of Tokyo,7-3-1, Hongo, Bunkyo-ku, Tokyo 113, Japan*

[b] *CERN, PS Division, 1211 Geneva 23, Switzerland*

Abstract

A novel system to monitor the intensity and the stability of a bunched beam of $\simeq 1.2 \times 10^7$ antiprotons ($\bar{p}$s) with a length of $\simeq 250$ ns (FWHM) and to measure its trapping efficiency in a Penning trap is described. This system operates parasitically detecting the pions from the annihilation of part of the beam in a degrader.

Six plastic scintillators have been coupled from one side to six proximity focused HPDs without preamplifiers and operating in current mode. This device works in the stray field of the ATHENA magnet with no loss of efficiency; the gain can be varied from zero to a few thousands with a precision better than 0.1% and the dynamic range is larger than 8 orders of magnitude. Linearity and stability have been measured up to charge responses of 100 nC, corresponding to the beam completely dumped. The beam counter has been calibrated in two different and independent ways giving consistent results.

Keywords: HPD, Scintillator, Beam Detector
PACS : 29.40.G; 20.40.M; 85.60.Dw; 85.60.Gz

1 Introduction

The goal of the ATHENA (ApparaTus for High precision Experiments on Neutral Antimatter) [1] experiment at CERN, is to produce and store low energy anti-hydrogen atoms ($\bar{H}$s). The 1S-2S transition can be excited resonantly and compared with that of the hydrogen atom (H) to a high precision [2]. Any difference may be due either to CPT violation or to an anomalous red shift originated by a different gravitational interaction of antimatter [3].
A bunched beam of $\simeq 1.2 \times 10^7$ $\bar{p}$s with a length of $\simeq 250$ ns (FWHM) and a

[1] Corresponding author. Tel.:+41-22-7674834, fax: +41-22-7678955
e-mail: Marco.Marchesotti@cern.ch

momentum of 100 MeV/c delivered by the Antiproton Decelerator (AD) [4] is degraded before entering a multi-ring Penning trap. Only $\simeq 0.1\%$ of the beam is trapped, cooled to sub-eV level by electron cooling [5] and accumulated. At the same time $\simeq 10^8$ low energy positrons (e^+s), emitted by a ^{22}Na source, are slowed down, trapped and accumulated in another trap.
One of the major challenges will consist in bringing $\bar{p}$s and e^+s in close contact to allow their recombination in a nested Penning trap [6]. Once $\bar{p}$s and e^+s are recombined, the confinement by electric forces ceases and the $\bar{H}$ would escape, hit the nearest wall and annihilate.
To confine the produced $\bar{H}$, the use of magnetic gradients interacting with the $\bar{H}$'s magnetic moment is investigated for the second phase.

2 The Beam Detector

The ATHENA beam line is sketched in fig. 1: the injected $\bar{p}$s travel inside a

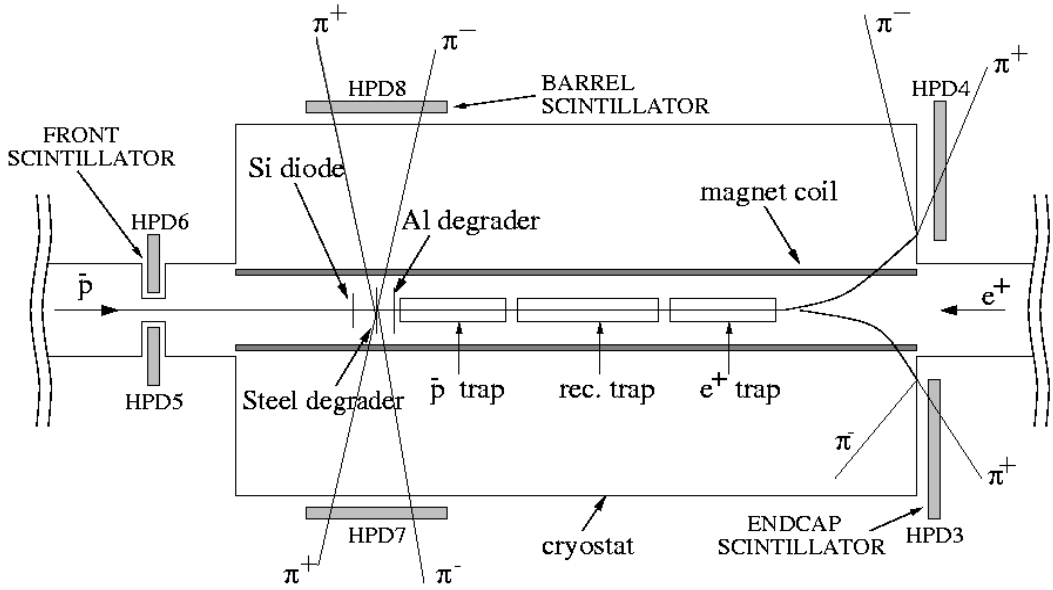

Fig. 1. Schematic upper view of the beam line setup; the scintillators are shown together with the name of the HPDs to which they are coupled. HPD7 and 8 have a window diameter of 25 mm, while the other ones of 18 mm (see later in par. 3).

solenoidal magnetic field of 3 T and are degraded by $25\,\mu m$ of stainless steel put 10 cm in front of the $\bar{p}$ catching trap and by $130\,\mu m$ of Al put on the first electrode of the same trap. The degraders further slow down the beam in order to have a better trapping efficiency; the possibility to use only one gas degrader to have more flexibility is under study.
A $67\,\mu m$ thick Si diode segmented in 5 pads, located 15.5 cm before the $\bar{p}$

trap, measures the beam position just before the entrance window of the trap. The beam transmission of the Si diode is $\simeq 100\,\%$.
On the basis of a Monte Carlo simulation, a trapping efficiency of $\simeq 0.1\%$ is expected with $\simeq 50\%$ of the beam that annihilates on the degraders and the remaining $\simeq 50\%$ with energy higher than $(5 \div 10)$ keV, corresponding to the highest trapping potential, that escapes from the trap and travels until the end of the cryostat where it annihilates.
A beam detector is necessary to monitor the beam intensity and the beam stability, to detect possible losses of $\bar{p}$ along the beam pipe and to measure the $\bar{p}$ trapping efficiency. Such a device is supposed to detect the pions coming from the annihilation of the $\bar{p}$s in the degraders, on the end of the cryostat and, eventually, in the beam pipe. Being the rate of the pions very high ($\simeq 10^{14}$ Hz), the beam detector can't operate in pulse mode counting the single particles: hence the current mode operation, measuring the total charge generated by the pions in the active volume during every shot, is necessary. To fulfil all these tasks, the beam detector must be stable and linear to high intensities and over a wide dynamic range; furthermore a good flexibility is required until the beam features are completely understood.

2.1 Scintillator layout and assembling

The beam detector consists of 3 systems each of 2 modules of plastic scintillator Bicron BC408 (with peak emission wavelength of 425 nm). The 3 systems, referred to as FRONT, BARREL and ENDCAP, are sketched in fig. 1 while their dimensions are reported in table 1.

Scintillator System	Length (cm)	Width (cm)	Thickness (cm)
FRONT	20.0	10.0	1.0
BARREL	80.0	20.0	1.0
ENDCAP	39.5	20.0	1.0

Table 1
Dimensions of the 3 scintillator systems.

All the scintillators are glued to lucite light guides from one side, wrapped with aluminized mylar sheets, sealed with black paper and coupled with optical grease (BICRON BC-630) to the photo-detector.
Every scintillator is equipped with a blue LED (with peak emission wavelength 423 nm) glued in a drilled hole in the middle of the scintillator side facing the light guide. The LED can be driven by a pulser (LeCroy 9212) to test the photodetector.
The ENDCAP scintillators were not used in the first run.

2.2 Photo-detector choice

The number of collected photons, produced in a 1 cm thick plastic scintillator by the charged pions coming from the annihilation of the beam, is given by:

$$n_\gamma = \delta \, n_{\bar{p}} \, \bar{n}_\pi \, \Omega \, k \, \epsilon \tag{1}$$

where δ is the percentage of dumped beam, $n_{\bar{p}} \simeq 1.2 \times 10^7$ $\bar{p}$s/shot is the nominal beam intensity, $\bar{n}_\pi = 3.5$ is the mean number of charged pions produced in a $p\bar{p}$ annihilation at rest, Ω is the solid angle covered by the scintillator, $k \simeq 1.5 \times 10^4$ γ/cm×MIP is the mean number of photons emitted by a $1\,cm$ thick plastic scintillator traversed by a MIP and ϵ is the light collection efficiency of the light guide. Assuming to dump half of the beam in the degraders and assuming $\Omega \simeq 10\%$ and $\epsilon = 50\%$, we obtain $n_\gamma \simeq 1.6 \times 10^{10}\,\gamma$/shot: with such an intensity any photomultiplier tube would saturate for the effect of the high density space charge. For example, the PMT XP2020 saturates with an intensity of $\simeq 4 \times 10^5\,\gamma/200$ ns [7], around 4 orders of magnitude below our working intensity. Furthermore the PMTs are very sensitive to external magnetic fields and their response is a complex function of the orientation with respect to the field lines.
A second choice would be to couple the scintillator directly to a Si photo diode: assuming a quantum efficiency QE $\simeq 40\%$, the number of photoelectrons (PEs) would be $n_{PE} \simeq 6.4 \times 10^9$ PEs and the corresponding charge $\simeq$ 10 nC (collected in $\simeq 250$ ns). This result would be obtained in the best case: if we take into account a realistic beam variation of a factor 2 in width, of a factor 5 in intensity (both achievable in the coming years' runs) and a variation in the dumping power between 10^{-1} and 2 (corresponding respectively to a beam transmission of 5% and to a full dumped beam), we would obtain a variation of a factor x, with $10^{-2} \leq x \leq 20$. In this situation a preamplifier is required to detect the low level signals; furthermore a high dynamic range ($\simeq 60$ dB) is necessary in order to maintain the linearity.
The optimal solution would be a Si diode without preamplifier, to not deteriorate the linearity and the dynamic range of the Si, but with a further adjustable linear gain of a few hundreds: the proximity focused Hybrid Photo Diode (HPD).

3 The HPD

The proximity focused HPD [8–12] is a vacuum tube in which the dynodic ladder is eliminated and the collection electrode is replaced by a planar Si diode biased in inverse mode. The working principle of the HPD is schematically shown in fig. 2: a PE, extracted from the photo cathode (PC), is accelerated by

a negative high voltage (-HV) towards a Si chip where it penetrates dissipating its energy creating one electron-hole (e-h) pair every 3.62 eV of released energy. Since the nature of the gain is dissipative rather than multiplicative, the HPD turns to be a linear device with a wide dynamic range and its gain is described by the following equation:

$$G = \frac{(HV - V_{th})\, q_e}{E_{ion}} \tag{2}$$

where V_{th} is a voltage threshold, q_e is the electron charge and $E_{ion} = 3.62$ eV is the Si ionization energy. The threshold is due to a passive Al layer deposited on the Si in order to improve the charge collection and the response uniformity. Applying a HV of $\simeq$ -15 kV a gain of $\simeq$ 3500 can be achieved: this is low if compared to that of a PMT ($\simeq 10^7$) and a further amplification is necessary in common applications where low light yields are available [13–15]. In this application, for which a large amount of light is available, the idea is to use a HPD, not preamplified, to have a wide dynamic range.
We have used two different models of proximity focused HPDs built by DEP [16]: one for the FRONT and the ENDCAP scintillators (model PP0350F) and the other for the BARREL scintillators (model PP0350D). In table 2 are reported the main characteristics of the two models.

Model	Window Diameter	Max HV	Capacitance	Max Bias
PP0350F	18. mm	-15 kV	120 pF	-130 V
PP0350D	25. mm	-8 kV	200 pF	-90 V

Table 2
Main characteristics of the used HPDs.

In both the models an S20-UV PC with a QE of 20% at 423 nm is deposited on the window in front of a 300 μm thick Si PiN diode in the E-type configuration. The 18 mm diameter HPDs are the same used in the FINUDA experiment: a full description of their characterisation can be found in ref. [13]; the 25 mm diameter HPDs have been chosen for their bigger surface, in order to improve the light collection efficiency.

3.1 Static characterisation

For each HPD the threshold V_{th} has been measured pulsing the LED with a fixed current and recording the signal pulse height corresponding to different HV values. In fig. 3 are reported the results for HPD5 (left) and HPD7 (right): the experimental points have been fitted with a straight line from -3.0 kV to -7.0 kV whose crossing point with the x axis gives the threshold (V_{th}). From the fit we found $V_{th} = (-2.21 \pm 0.05)$ kV for HPD5 and $V_{th} = (-1.66 \pm 0.05)$

kV for HPD7. Once the thresholds are known, the gain can be rescaled for different HV operating values.
The noise of the HPDs coupled to the scintillators is 0.4 mV (rms), corresponding to 2 pC. Since signals ranging from a few hundreds of mV to a few tens of V are expected, all the measurements can be considered with virtually no noise.

3.2 Behaviour in an external magnetic field

No response variation is expected if the magnetic field and the electric field generated by the HV are parallel, otherwise the PEs are accelerated along a spiral which loops around the magnetic field lines. The PEs still reach the Si surface with full energy but in a displaced position and with variable impinging angle: no signal cutoff is expected unless the PEs are dragged outside the Si chip. As the impinging angle increases the dead contact layer on the Si chip becomes difficult to penetrate and the signal is expected to decrease with increasing magnetic field.
Intensive studies of behaviour of a proximity focused HPD in an external magnetic fields have been performed [11].
We measured the response of the HPDs in the ATHENA magnetic field using a pulsed LED, hold in front of the PC's centre by a plastic support fixed to the HPD. We also measured the field intensity with a portable gauss-meter.
A great care was taken in choosing a position of the HPDs so that the field intensity was less than 1 kG and the angle with respect to the HPD electric field was less than 30^o (though it was not easy to measure with good precision the intensity and the direction of the field) where no losses are foreseen [11].
The pulse height of the signal extracted from the HPDs was measured with a digital scope (LeCroy 9354A). The measurement was repeated with the magnetic field switched off: the difference between the two measurements was compatible with zero within 3%. The difference are mainly due to the LED movements during the measurements, due to the home made setup.
Also the threshold was measured with and without magnetic field and no variation was found within the errors (3%).

3.3 Power supply

The HV from the power supply (Heinzinger HNC 30 kV-20 mA) has been filtered by a π-filter with two capacitors of 100 nF and a resistor of 100 kΩ and then sent to the PC through a $4\,m$ long coaxial cable (Nokia Kabel-HTC-50-2-1 FRNC 95/30). A big care was taken in the insulations of the high voltage contacts, mostly performed with teflon shields.

The bias voltage of each HPD diode has been filtered and distributed by a small bias circuit, sketched in fig. 4, mounted on the back side of each HPD.

4 First results

AD delivered the first $\bar{p}$s from November 30-th, 1999 for 3 days: during this run the electron cooling was not optimised and the beam intensity was $\simeq 10^3\,\bar{p}$s/shot, 3 to 4 orders of magnitude reduced compared to the nominal one. A prototype of the beam detector was tested to check its feasibility and its reliability: it consisted of 2 BARREL scintillators, each coupled to both sides to two 18 mm diameter HPDs, one (BARREL1) aligned with the Al degrader, the other (BARREL2) positioned $\simeq 2$ m downstream far from the $\bar{p}$ injection region. The signals extracted from the HPDs were directly fed into a digital scope (LeCroy model 9354A) triggered by the AD extraction signal. The HV was set to -15 kV and the bias to -120 V.
In fig. 5 are shown some typical signals from the HPDs: the waveforms 3 and 4 come from the BARREL1 scintillator, the waveforms 1 and 2 from the BARREL2. The attenuation of the signals 1 and 2 with respect to 3 and 4, is due to the low $\bar{p}$ transmission of the degrader. All the signals are well correlated in time: the bunch length is $\simeq 500$ ns (FWHM). The charge collected by the HPDs 3 and 4 is $\simeq 40$ pC, corresponding to $3.6 \times 10^2\,\bar{p}$s, in accordance with the beam intensity if we take into account that part of the beam was lost in the beam pipe because of the beam blow up for the not optimised electron cooling.
From these measurements we deduced that the HPD in this configuration without preamplifier could be used as photo detector for the beam counter and that it was a flexible device: in fact we were able to detect a signal a factor $\simeq 10^3$ lower than the nominal one, increasing the HPD gain by the same amount.

5 Relative calibration and trapping efficiency

From a Monte Carlo simulation the best trapping efficiency ($\simeq 0.1\%$) is obtained when half of the beam annihilates on the degraders and the remaining escapes the trap and annihilates at the end of the cryostat. The trapping efficiency can be optimised and monitored very precisely in future with a variable degrader. The beam will be fully stopped: in this case the ratio between the charge measured by the BARREL system over the ENDCAP will show a maximum; the opposite situation will be measured with a fully transmitted beam. These measurements will give the two extreme points of a full dumped beam

and of a full transmitted beam: the working point, corresponding to the best trapping efficiency, will be most likely in the middle. It must be stressed that no absolute calibration is necessary for this measurement, because only charge ratios are involved. A fine tuning can be done by dumping the trapped $\bar{p}$s on the Al degrader by inverting the trap potential and then counting the charged pions from their annihilation with a scintillator coupled to fast PMTs. Once the best settings are found, the intensity can be monitored in parasitic way shot by shot as described before.

6 Absolute calibration

The beam detector cannot be calibrated with a radiation source, because the HPD, in this configuration, is not sensitive to single particle counting.
An absolute calibration has been performed with an Activation Method (AM) and a Schottky Method (SM), described in the following, using the experimental setup sketched in fig. 6.

Two scintillators were calibrated: a FRONT one (coupled to HPD6), and a BARREL one (coupled to HPD7) positioned with their centres aligned with the beam line; the solid angles covered by the FRONT and the BARREL scintillators are respectively $\Omega_{FRONT} = 23.7\%$ and $\Omega_{BARREL} = 24.1\%$.
The HV of the HPDs was set to -2.5 kV and the bias to -70 V.
In fig. 7 is reported the layout of the DAQ chain used for the test.

The signal from the HPDs was attenuated by 38 dB and then split with a linear fan-in-fan-out: one end was sent to the scope, the other one was further attenuated by 35 dB for HPD6 and by 29 dB for HPD7 and finally fed into an ADC (LeCroy model 1182) with a charge resolution of 50 fC. Both the scope and the ADC were triggered by the AD warning signal.
The ADC data were transfered to a personal computer via a VME/MXZ bus, while the scope data were readout via GPIB and both recorded on a disk. The number of $\bar{p}$s was measured for each shot before the extraction by a low noise Schottky pickup (SP) [17,18], with a sensitivity of $\simeq 1\%$.
The beam was fully dumped by an Al foil, positioned at the entrance of the ATHENA beam pipe, as shown in fig. 6. A typical signal from HPD7 acquired with the scope is reported in fig. 8: the pulse height is -20.60 V (over 50 Ω), the collected charge is 100.84 nC and the width is 246.1 ns (FWHM). The waveform follows accurately the longitudinal bunch shape generated by the RF system.
A total of 32 shots was acquired in 1h 46s: for 3 of these, no beam was ejected from AD, for other 9 the number of ejected $\bar{p}$s was not recorded due to a problem in the Schottky DAQ; for these events the number of $\bar{p}$s was extrapolated from the charge by rescaling it with respect to the other ones.

In fig. 9 the histograms of the ADC counts (divided by the attenuation factors) of HPD6 (left, solid line), of HPD7 (left, dashed line) and of their correlation (right) are reported.

The mean number of ADC counts (corrected for the attenuation factors) is $(3.28 \pm 0.07) \times 10^6$ ADC counts for HPD6 and $(1.57 \pm 0.03) \times 10^6$ ADC counts for HPD7.

6.1 Activation Method

This method relies on the following activation process, studied in LEAR [19]:

$$\bar{p} + Al \rightarrow^{24} Na^* \tag{3}$$

$$^{24}Na^* \rightarrow^{24} Na^* + \gamma \tag{4}$$

The branching ratio of reaction (3) is $BR = (2.1 \pm 0.3)\%$, while that of reaction (4) is $BR = 100\%$. The half life of $^{24}Na^*$ is $T_{\frac{1}{2}} = 15$ h and the γ ray can be emitted with two different energies: $E_1 = 1369$ keV and $E_2 = 2754$ keV.
The basic idea is to dump all the beam extracted from the AD on an Al foil and, after the irradiation, to measure the induced activity counting the γs from reaction (4) from which the beam intensity can be derived.
Four Al sheets, each with a thickness of $110\,\mu m$, were sticked together and placed in vacuum; other sheets were placed around the valve to measure the background.
The activity induced by the beam in the Al sheets, was measured with a Ge detector at a distance of 4.0 cm and at 24.0 cm from the Al foil and then extrapolated to the end of the irradiation time: the results are reported in table 3.

	Distance (cm)	Activity (Bq)
Measurement 1	4.0	84.0 ± 4.7
Measurement 2	24.0	92.7 ± 7.4
Background	4.0	0.0

Table 3
Measured activities of the Al foil extrapolated to the end of the irradiation.

The beam intensity can be derived from the measured activity making use of the following equation [19]:

$$\sum_{i=0}^{N} A_i = \sum_{i=0}^{N} \frac{n_i^{\bar{p}} P}{\tau}\, e^{-\frac{t_M - i\bar{t}}{\tau}} \tag{5}$$

where $N = 32$ is the number of shots, A_i is the activity induced in the Al foil by the i-th shot, $n_i^{\bar{p}}$ is the number of $\bar{p}$s of the i-th bunch, t_M =1h 46s is the duration of the irradiation, $\bar{t}$ =118 s is the inter-bunch time, $P = (2.1 \pm 0.3)\%$ is the activation probability of reaction (3), τ is the mean lifetime of $^{22}Na^*$. Assuming a uniform activation induced by every shot, approximating $e^{\frac{i\bar{t}}{\tau}} \simeq 1 + \frac{i\bar{t}}{\tau}$ and taking into account that the shots number 18, 19 and 30 came without beam, the integrated number of $\bar{p}$s, $n_{\bar{p}}^{tot} = \sum_i n_i^{\bar{p}}$, and the mean number of $\bar{p}$s per shot have been calculated and the results are reported in table 4.

Activity	Integrated number of $\bar{p}$s	Mean number of $\bar{p}$s/shot
(84.0 ± 4.7) Bq	$(3.416 \pm 0.180)\, 10^8$	$(1.101 \pm 0.062)\, 10^7$
(92.7 ± 7.4) Bq	$(3.523 \pm 0.281)\, 10^8$	$(1.215 \pm 0.097)\, 10^7$
Combined	$(3.477 \pm 0.244)\, 10^8$	$(1.199 \pm 0.084)\, 10^7$

Table 4
Integrated number of $\bar{p}$s and mean number of $\bar{p}$s/shot calculated from the corresponding measured activity.

The combined result is the weighted mean of the measurements taken at the two different distances weighted with the distance.

6.2 Schottky Method

This method relies on the direct measurement of the number of $\bar{p}$s inside the AD ring before the electron cooling at 100 MeV/c and before the ejection by means of the SP [17]. The electron cooling efficiency has been measured by rebunching the beam in harmonic 3 (where the SP is more sensitive at 100 MeV/c) before the ejection and it was $\simeq 100\%$. The total number of $\bar{p}$s is $(3.618 \pm 0.114)\, 10^8$, while the mean number of $\bar{p}$s per shot is $(1.248 \pm 0.039)\, 10^7$.

6.3 Comparison between the AM and the SM

The calibration factors obtained with the AM and with the SM (with the ADC counts normalised to the solid angle) are reported in table 5.

The results are compatible within the errors and show that an absolute calibration is possible at the level of 7.3% for the AM and of 3.8% for the SM. The calibration performed with the SM is twice more accurate, being the sensitivity of the SP very high ($\simeq 1\%$) at these intensity. On the other hand the number of $\bar{p}$s is measured inside the ring before the electron cooling process at 100 MeV/c and before the extraction and so possible cooling inefficiencies

Calibration Method	HPD6 (ADC counts/$\bar{p}$)	HPD7 (ADC counts/$\bar{p}$)
Activation (84.0 Bq)	1.257 ± 0.076	0.592 ± 0.035
Activation (92.7 Bq)	1.139 ± 0.094	0.536 ± 0.044
Activation (combined)	1.154 ± 0.084	0.543 ± 0.039
Schottky	1.109 ± 0.042	0.522 ± 0.019

Table 5
Calibration factors obtained with the AM and SM.

and losses in the ejection line are not taken into account. For these reasons the AM is more reliable than the SM, at least in this experimental situation, because the number of $\bar{p}$s is measured at the end of the ejection line, even if with a worse error. A better calibration with the SM will be possible next year when the ejection line will be equipped of a low noise SP to measure directly the beam intensity after the extraction.

7 Full dumped beam test

A second test with the beam completely dumped was performed to measure the HPD response to a large amount of light and to perform an absolute calibration with the SM. The used experimental set up is shown in fig. 10: the FRONT scintillators, coupled to HPD5 and HPD6, and the BARREL ones, coupled to HPD7 and HPD8 were used. The solid angles covered by a FRONT scintillator is 6.2%, that by a BARREL one is 0.49%. The PC high voltage was set at -4 kV and the bias at -80 V; the signals from the HPDs were attenuated by a total of 61 dB for HPD5 and HPD6, and by 35 dB for HPD7 and HPD8. In fig. 11 are reported the signals directly extracted from the diode's output and sent to the scope: they are correlated in time and follow the longitudinal beam structure. The long tail on the trailing edge of the signals from HPD5 and HPD6 maybe due to the screening of the bias field by the large charge generated in the Si chip (plasma effect). The tail effect is of $\simeq 10\%$ and all the charge is completely collected in $\simeq 1.5\,\mu s$. This tail can be eliminated using a higher bias voltage. No trace of saturation is evident from HPD7 and HPD8: in this case the charge generated is much smaller.
A detailed study of the waveforms could be useful in the future to monitor the beam quality in parasitic mode.
In fig. 12 the histograms of the ADC counts (divided by the attenuation factors) of HPD5 (left, solid line), of HPD6 (left, dashed line) and their correlation plot are reported.

The mean number of ADC counts (corrected for the attenuation factors) is $(1.87 \pm 0.03)\,10^6$ ADC counts for HPD5 and $(0.078 \pm 0.001)\,10^6$ ADC counts

for HPD6.
A calibration with the SM of the FRONT system gave the following results: (2.02 ± 0.11) ADC counts/$\bar{p}$ for HPD5 and (1.60 ± 0.05) ADC counts/$\bar{p}$ for HPD6 (the number of ADC counts is normalised to the solid angle). A cross check with the previous calibration, by rescaling the solid angles and the HPD gain, is consistent within 4.5%.

8 Future plans

In the 2001 run all the 6 scintillators shown in fig. 1 will be used: the FRONT ones to detect possible beam losses, especially during the steering of the extraction line, the BARREL ones to monitor the beam intensity parasitically and the ENDCAP ones to measure the trapping efficiency when the variable degrader will be ready.
Once the ejection line will be equipped with the new SP, a more precise calibration will be done with the SM.
A detailed study of the HPD's waveforms will be useful in further understanding the characteristics of the beam and to improve its quality, a crucial item for the ATHENA physics.

9 Conclusions

The beam detector of the ATHENA experiment has been described: it consists of 6 plastic scintillators, each coupled from one side to a proximity focused HPD without preamplifier. This system, after a calibration, has been used to monitor parasitically a bunched beam of $\simeq 1.2 \times 10^7$ $\bar{p}$s with a width of $\simeq 250$ ns (FWHM), to detect possible losses in the beam pipe and to measure the $\bar{p}$ trapping efficiency. This detector is linear and stable up to charge responses of $\simeq 100$ nC and it works with no loss of efficiency in the stray field of the ATHENA solenoid. It is a reliable device, giving the opportunity to vary its gain from zero to a few thousands without any change neither in detection efficiency, nor in linearity.
It is the first time that a HPD is used without preamplifier, taking advantage of the huge amount of light, to exploit its huge dynamic range.

10 Acknowledgements

We wish to thank prof. P. Benetti of the University of Pavia and V. Filippini of the INFN of Pavia for their interesting discussions during the project phase, S. Bricola and C. Marciano of the INFN of Pavia who built all the mechanics, prof. A. Rotondi of the University of Pavia and D. Grassi of the INFN of Pavia who helped us in the setting up of the detector and in its characterisation.

References

[1] M.H. Holzscheiter et al., *Antihydrogen Production and Precision Experiments*, **CERN/SPSLC 96-47, SPSLC/P302**, October 20, 1996.

[2] M. Charlton et al.; *Phys. Rep.* **241** (1994) 65.

[3] R.J. Hughes, M.H. Holzscheiter; Journal of Modern Optics **39** (1992) 263.

[4] S. Baiard et al., *Design Study of the Antiproton Decelerator: AD*, **CERN/PS 96-43 (AR)**, November 1996.

[5] M.H. Holzscheiter et al.; *Phys. Lett.* **A214** (1996) 279.

[6] M.H. Holzscheiter et al.; *Phys. Lett.* **A129** (1998) 38.

[7] PHILIPS data sheets.

[8] R. DeSalvo, *CLNS* **82-92** Cornell University, Ithaca, 1987.

[9] L.K. van Geest et al., *Nucl. Instr. and Meth. A* **310** (1991) 261-266.

[10] R. DeSalvo et al., *Nucl. Instr. and Meth. A* **315** (1992) 375-384.

[11] H. Arnaudon et al., *Nucl. Instr. and Meth. A* **342** (1994) 558-570.

[12] G. Anzivino et al., *Nucl. Instr. and Meth. A* **365** (1995) 76-82.

[13] V. Filippini et al., *Nucl. Instr. and Meth. A* **424** (1999) 343-351.

[14] E. Albrecht et al., *Nucl. Instr. and Meth. A* **411** (1998) 249-264.

[15] P. Cushman et al., *Nucl. Instr. and Meth. A* **387** (1997) 107-112.

[16] Delft Electronische Producten, Dwazziewegen 2, NL-9300 AB Roden, The Netherlands.

[17] C. Gonzales et al., *An ultra low-noise AC beam transformer for deceleration and diagnostics of low intensity beams*, **PAC '99, NY**, 1999.

[18] M.E. Angoletta et al., *The new digital receiver based system for antiproton beam diagnostics*, **CERN/PS 2001-044 (BD)**.

[19] P. Lubinski et al., *Phys. Rev. Lett.* **73**, 3199 (1994).

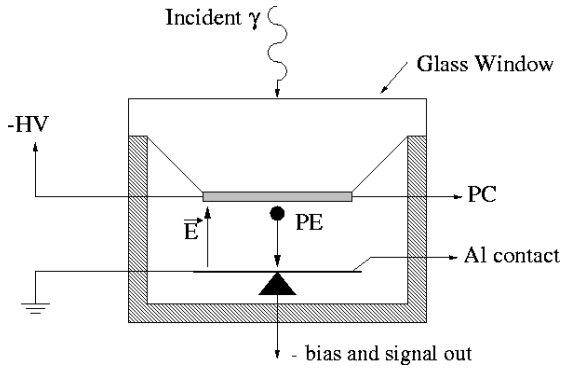

Fig. 2. Schematic working principle of the HPD.

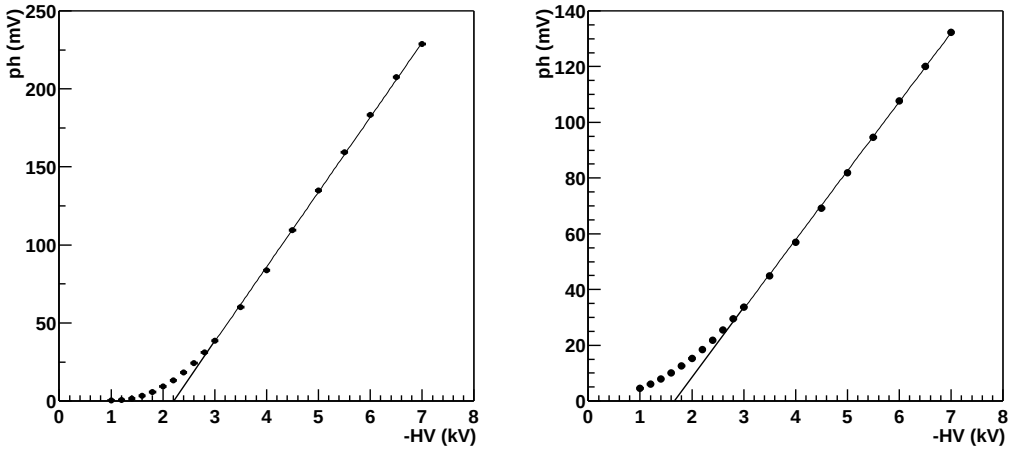

Fig. 3. Signal pulse height versus high voltage for HPD5 (left) and HPD7 (right). The intercepts with the x axis gives the threshold V_{th}.

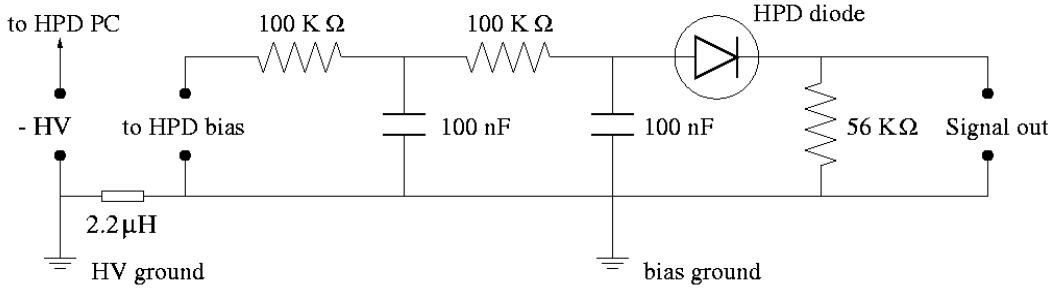

Fig. 4. Wire diagram of the bias supply circuit.

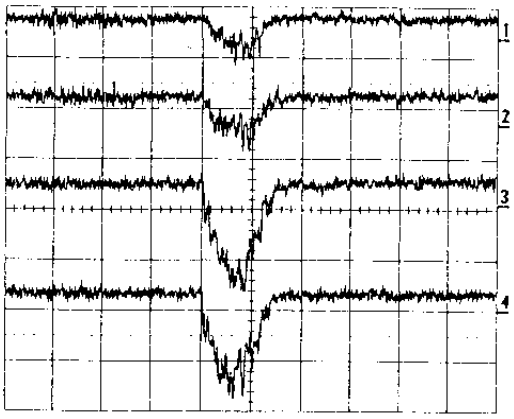

Fig. 5. First signals detected by the beam counter prototype. The horizontal pitch is 500 ns/division and the vertical one is 2 mV/division.

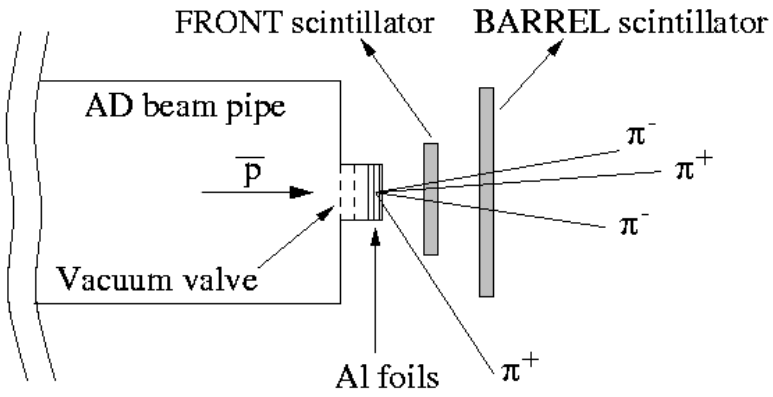

Fig. 6. Schematic upper view of the setup used for the absolute calibration.

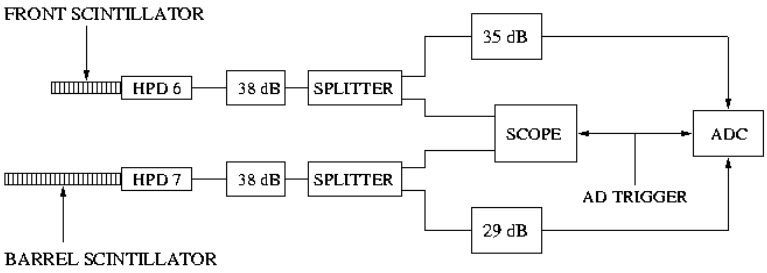

Fig. 7. Layout of the DAQ chain used for the absolute calibration.

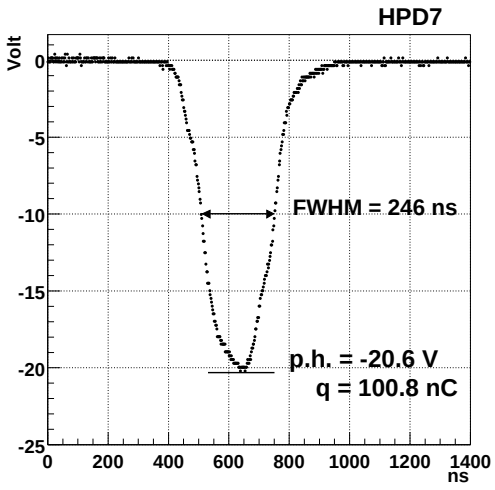

Fig. 8. Typical waveform from HPD7.

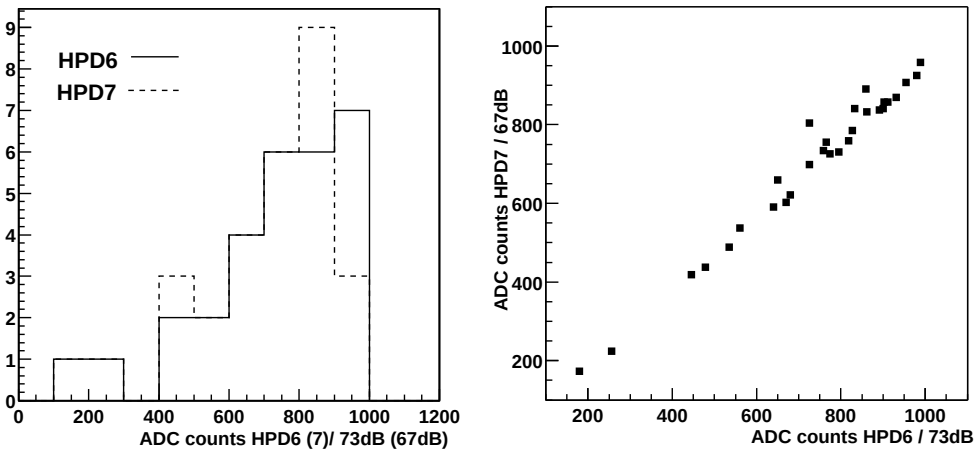

Fig. 9. Histograms of the ADC counts (divided by the attenuation factors) of HPD6 (left, solid line), HPD7 (left, dashed line) and their correlation (right).

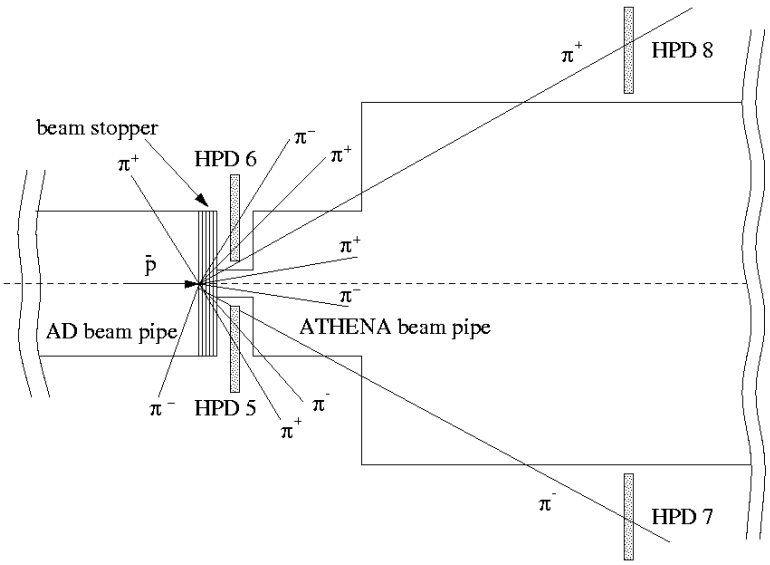

Fig. 10. Schematic upper view of the setup used for the full stopped beam tests.

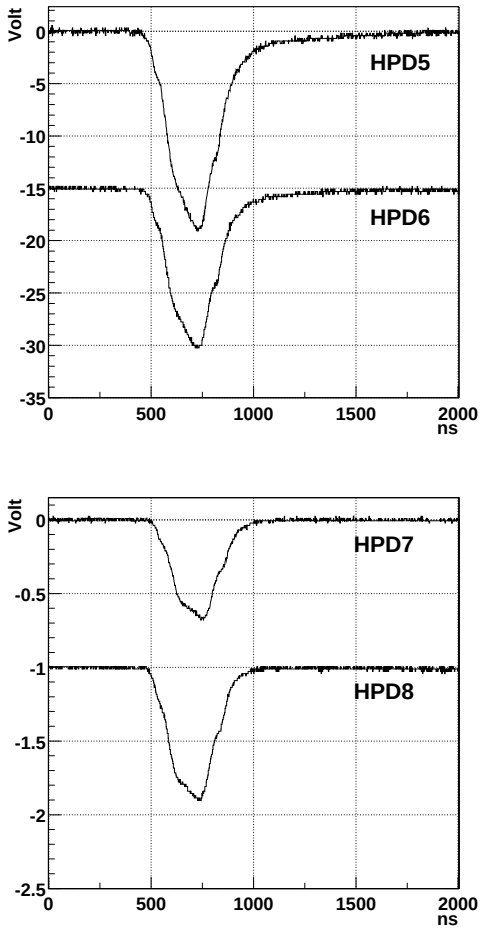

Fig. 11. Signals extracted from the HPDs with the beam completely dumped.

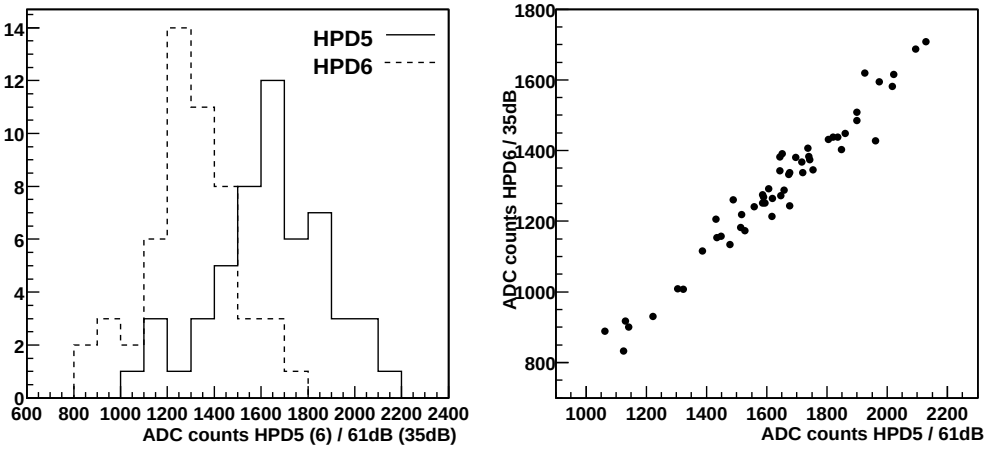

Fig. 12. Histograms of the ADC counts (divided by the attenuation factors) from HPD5 (left, solid line), HPD6 (left, dashed line) and their correlation (right).